ELSEVIER

Spectrochimica Acta Part B 52 (1997) 657–666

SPECTROCHIMICA ACTA PART B

Investigations on nanosecond laser produced plasma in air from the multi-component material $YBa_2Cu_3O_7$

Geetha K. Varier, Riju C. Issac, S.S. Harilal, C.V. Bindhu, V.P.N. Nampoori*, C.P.G. Vallabhan

Laser Division, International School of Photonics, Cochin University of Science and Technology, Cochin 682 022, India

Received 21 May 1996; accepted 14 October 1996

Abstract

The laser produced plasma from the multi-component target $YBa_2Cu_3O_7$ was analyzed using Michelson interferometry and time resolved emission spectroscopy. The interaction of 10 ns pulses of 1.06 μm radiation from a Q-switched Nd:YAG laser at laser power densities ranging from 0.55 GW cm^{-2} to 1.5 GW cm^{-2} has been studied. Time resolved spectral measurements of the plasma evolution show distinct features at different points in its temporal history. For a time duration of less than 55 ns after the laser pulse (for a typical laser power density of 0.8 GW cm^{-2}), the emission spectrum is dominated by black-body radiation. During cooling after 55 ns the spectral emission consists mainly of neutral and ionic species. Line averaged electron densities were deduced from interferometric line intensity measurements at various laser power densities. Plasma electron densities are of the order of 10^{17} cm^{-3} and the plasma temperature at the core region is about 1 eV. The measurement of plasma emission line intensities of various ions inside the plasma gave evidence of multiphoton ionization of the elements constituting the target at low laser power densities. At higher laser power densities the ionization mechanism is collision dominated. For elements such as nitrogen present outside the target, ionization is due to collisions only. © 1997 Elsevier Science B.V.

Keywords: Laser plasma interaction; Laser produced plasma; Michelson interferometry; Plasma ionization

1. Introduction

With the advent of high power pulsed lasers, the study of the interaction of light with matter has assumed a new dimension in the past three decades. The evaporation of a solid target by an intense laser pulse and the subsequent plasma formation has evoked much attention in both the basic and the applied research fields. Pulsed laser evaporation is a very effective and efficient method for the deposition of high quality thin films of semiconductors [1] and superconductors [2–7]. Also, the highly luminous plasma produced during and after laser–target interaction is a very rich source of ionic, atomic and molecular species and also of clusters of atoms [8–12].

Considerable efforts are being made worldwide in plasma diagnostics and in studying the dynamics of laser–target interactions [13–22]. Among the various plasma parameters, the plasma temperature and the plasma electron and ion densities are the main quantities that determine the plasma characteristics. There are various methods for obtaining these quantities, including laser interferometry [23], emission spectroscopy [24], Thomson scattering [25], laser induced fluorescence [26] etc. The evolution of these quantities with respect to the laser power density, the

* Corresponding author.

PII S0584-8547(96)01607-2

ambient pressure and the time can be used to characterize the various electronic and photonic processes taking place inside the plasma [27,28]. Nanosecond laser pulses which produces power densities up to 10^3 GW cm^{-2} interact in a distinctly different way compared with picosecond pulses, for which the power density ranges from 10^3 to 10^7 GW cm^{-2}. In the intense field of a picosecond laser pulse, various processes such as tunnel ionization [27] and the relativistic skin effect [29] etc. appear in addition to multiphoton ionization and collision induced ionization, whereas in the nanosecond regime the ionization inside the plasma is limited mainly to the two latter effects.

The present paper deals with studies on the interaction of a pulsed laser beam with the multi-component high T_C superconducting material $YBa_2Cu_3O_7$ in air at atmospheric pressure and at laser power densities ranging from 0.5 to 1.5 GW cm^{-2}, using Michelson interferometry and emission spectroscopy. In Section 2 we describe the experimental setup, and the results obtained are discussed in Section 3.

2. Experimental details

The experimental setup for electron density measurements using interferometry is as shown in Fig. 1. The sample chosen for our studies is a disc (1.75 cm diameter, 0.5 cm thickness) of $YBa_2Cu_3O_7$ (YBCO). An intensity stabilized 4 mW He–Ne laser (Spectra Physics, Model No. 102-4) is used as the light source for the Michelson interferometer. The beam in one of the arms of the Michelson interferometer grazes the sample surface. The shift in the fringe pattern is measured as a voltage change using a fast PIN photo diode (HP-4207, rise time 1 ns, quantum efficiency 0.71 electrons per photon, noise equivalent power < -108 dBm) and displayed on a 200 MHz digital storage oscilloscope (Iwatsu, Model DS 8621). All the measurements were made in a single pulse protocol in order to avoid the residual heating effect from the previous pulse. After a few measurements the target is rotated manually so that a fresh surface is available for ablation. High power laser radiation from a pulsed Nd:YAG laser (Quanta ray DCR 11, 30 MW peak power) at a wavelength of 1.06 μm with pulse duration 10 ns (FWHM) is focused using a convex lens of focal length 20 cm normal to the target in order to produce the plasma. The target is placed away from the focal point of the lens and the laser spot size is 7×10^{-2} cm in radius, which is measured from the etch pattern on a carbon film placed at the target position. The laser pulse energy is measured using a calibrated laser energy meter and the power density at the focal spot is calculated after reflection correction from the lens surfaces. The pulse energy is varied during the experiment by using suitable attenuators. The experiment was performed on an indigenously built vibration isolation table.

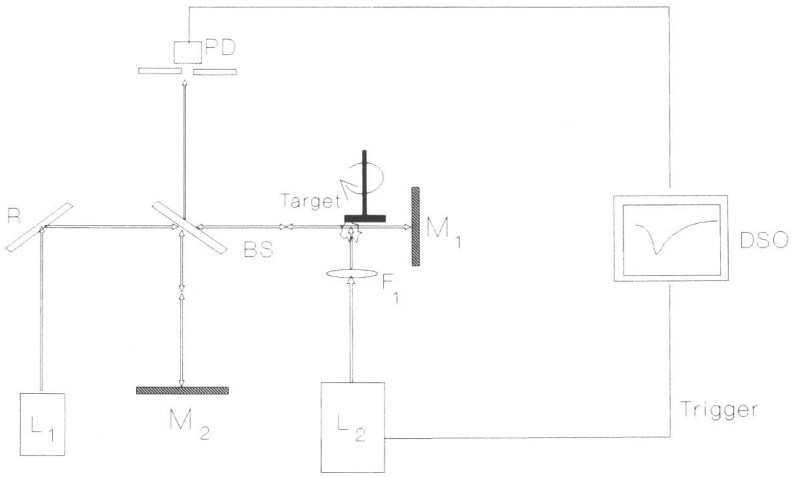

Fig. 1. Schematic diagram of the experimental setup. L_1, He–Ne laser; L_2, Nd:YAG laser; R, reflector; BS, beam splitter; M_1, M_2 concave mirrors; F_1, focusing lens; PD, photodiode; DSO, digital storage oscilloscope.

The schematic diagram of the experimental setup for the emission measurements is almost the same as the one described earlier, except for minor modifications [30]. Plasma is produced using the same Nd:YAG laser at a pulse repetition frequency of 10 Hz. The target was mechanically rotated and after every 5 min scan the target was shifted laterally in order to minimize the reduction in emission intensity due to surface pitting. The emission spectrum from the plasma was viewed perpendicular to its expansion direction by imaging the plasma plume using collimating and focusing glass lenses so that a 1:1 image of the plume was obtained at the entrance slit of a 1 m monochromator (SPEX model 1704 with entrance and exit slits parallel to the target surface, each having a width of 30 μm, grating with 1200 grooves per mm blazed at 5000 Å and spectral bandpass 0.1 Å). The scan rate of the monochromator was adjusted by using a microprocessor controlled scanning arrangement. A thermoelectrically cooled Thorn EMI photomultiplier tube (model KQB 9863, rise time 2 ns and quantum efficiency 22%) coupled to a boxcar averager/gated integrator (Stanford Research Systems, SR 250) triggered in phase with the start of the laser pulse was used for the detection and averaging of the plasma emission intensity. The boxcar averager gate width was set to 5 ns and intensities from ten consecutive pulses were averaged and then fed to the chart recorder. The recorded spectra were reproducible in wavelength and intensity.

3. Results and discussion

3.1. Time resolved plasma emission

The pulsed laser evaporation process can in general be classified into three separate regimes [13]: the interaction of the laser beam with the target material resulting in the evaporation of the surface layers; interaction of the evaporated material with the incident laser beam causing rapid ionization and plasma formation; and finally the rapid cooling of the plasma. The plasma evolution after the interaction of the high power laser beam with the target consists of two distinct domains in time. Initially there is a sudden increase in the emission intensity, and after attaining the peak intensity it decreases rapidly [31,32]. We have carried out time resolved spectral measurements in these two time domains with a view to deciphering the different heating, ionization, and cooling processes taking place inside the plasma. The time

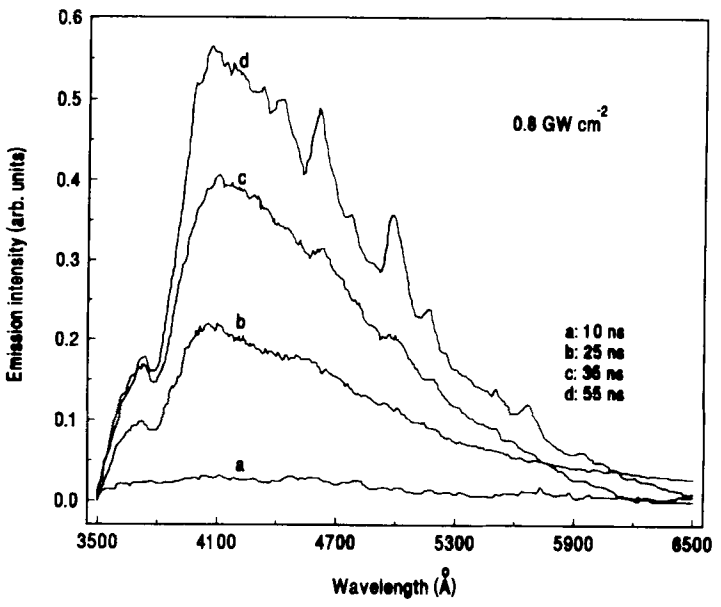

Fig. 2. Plasma emission spectrum in the wavelength range λ 3500–6500 Å at different time delays and at the typical laser power density 0.8 GW cm^{-2}; (a) 10 ns, (b) 25 ns, (c) 35 ns, and (d) 55 ns. The plasma continuum radiation peaks around 4100 Å.

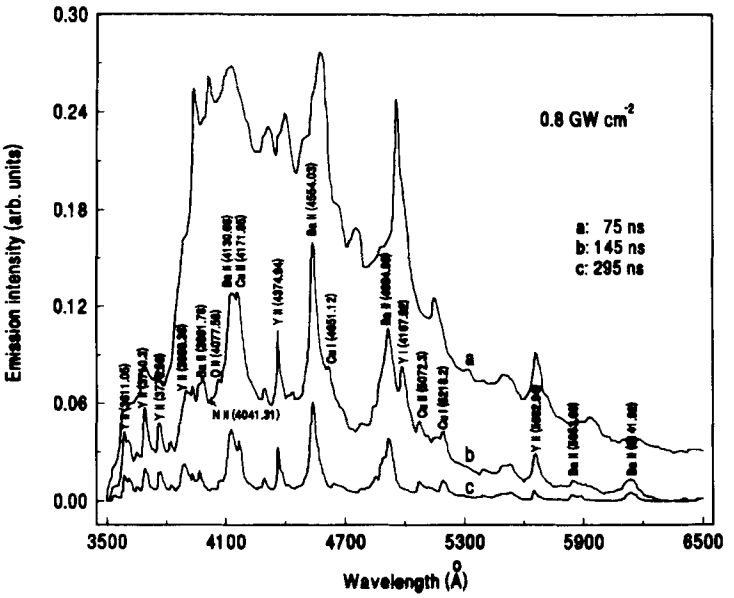

Fig. 3. Plasma emission spectrum in the wavelength range λ 3500–6500 Å at different time delays during plasma cooling at laser power density 0.8 GW cm^{-2}; (a) 75 ns, (b) 145 ns, and (c) 295 ns.

resolved emission spectra are given in Figs. 2 and 3, respectively, which clearly distinguish the different emission processes inside the plasma. At the initial stages of the plasma formation, which extend from 0 to ≈ 55 ns, there is an increase in the emission intensity. It should be noted that the time of 55 ns is significantly longer than the pulse duration. In this time span (0–55 ns), as seen from Fig. 2, the emission spectrum consists of the plasma blackbody radiation, without much line emission. In general, the main source of the plasma continuum is bremsstrahlung radiation and radiative recombination [34]. Thus, the shape of the spectrum shows the abundance of free electrons and ions inside the plasma during this period in its temporal history.

Beyond 55 ns, as shown in Fig. 3, the line to continuum intensity ratio increases, and finally, after about 150 ns, the spectrum consists mainly of emission lines corresponding to atomic and ionic species. It has also been observed that the emission lines are highly Stark broadened [35] during the initial stages of the plasma owing to very high plasma electron densities. The emission spectra obtained at different laser power densities are recorded, and it is seen that at relatively low power densities the spectrum represents mostly neutral and singly ionized species, whereas at higher laser power densities it contains lines corresponding to neutral and to singly and doubly ionized species. Lines corresponding to Ba(I), Ba(II), Y(I), Y(II), Cu(I), Cu(II), N(I), N(II), O(I) and O(II) and also some less intense lines from Ba(III), Y(III), Cu(III) and O(III) have been identified. The plasma emission lasts for a few microseconds.

3.2. Plasma electron density

The ablated material ejected from the target surface consists of ions, atoms and molecules in addition to free electrons. The atomic contribution to the refractive index is given by [36]

$$\mu_{at} = 1 + \frac{e^2}{8\pi^2 \epsilon_0 m} \sum_i \frac{N_i f_i}{(\nu_i^2 - \nu^2)} \quad (1)$$

where e is the electron charge, ϵ_0 is the permitivity of free space, m is the mass of electron, N_i is the number density of the lower level of a transition, f_i is the oscillator strength, ν_i is the atomic resonance line frequency and ν is the frequency of light used to make the observation. The above equation suggests that the contribution from the atomic refractivity is appreciable only near the resonance transitions. All

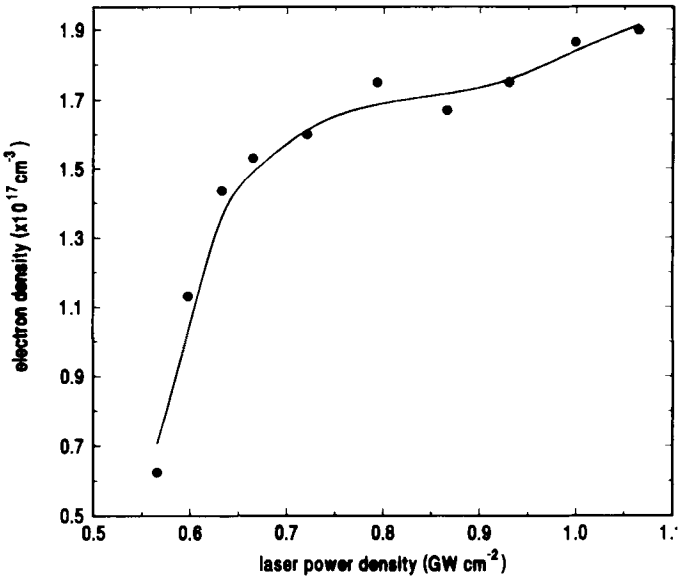

Fig. 4. Variation of the electron density as a function of the laser power density.

the resonance lines in the present plasma are sufficiently far from the probe wavelength λ. Hence the electron contribution to the refractive index dominates in the present measurements. The plasma electron density also peaks at a delay time of 55 ns (depending on the laser power density delivered to the target) and it is clear from the emission spectra in Fig. 2 that no other spectroscopic method can be used at smaller time delays for density measurements, as the spectrum is dominated by plasma blackbody radiation with the absence of line emission. The line averaged electron densities were calculated using the equation (see Appendix A)

$$\bar{n}_e \cong \frac{k\gamma(t)}{\lambda l} \tag{2}$$

Here $k \cong 1.778 \times 10^{12}$ cm^{-1}, $\gamma(t)$ is the phase difference due to the presence of the plasma, λ is the probe beam wavelength and l is the lateral extension of the plasma.

Fig. 4 represents the variation of the electron density with the laser power density. Even though the electron density is a function of time, the temporal profile of the electron density is not considered here. Instead, the peak electron density is plotted as a function of laser power density. The electron density ranges from 1×10^{16} cm^{-3} to 2.4×10^{17} cm^{-3} in the present power density range and exhibits a nonlinear relationship. The distinct regions of different slopes correspond to different mechanisms for the laser beam interaction with the plasma. Near 0.55 GW cm^{-2} rapid ionization causes surface damage of the sample. Above this damage threshold, there is a marked increase in the plasma electron density for power densities up to 0.65 GW cm^{-2}. Beyond this value the change in electron density seems to be more gradual up to 1.1 GW cm^{-2}. In the present case, as the plasma in air at atmospheric pressure is of high density, there will be large numbers of collisions among the particles. Owing to high electron–atom and electron–ion collision frequencies, the plasma can be regarded as obeying conditions of local thermodynamic equilibrium (LTE) [33]. The plasma electron temperature can be calculated from the ratio of the integrated line intensities [34] of elements at the same ionization level. It is found that the plasma temperature is (0.85 ± 0.05) eV after 300 ns from the beginning of the laser pulse.

3.3. Laser plasma interaction and ionization

In general, one can consider that the leading part of the laser pulse produces the plasma while the trailing part interacts with the plasma, resulting in intense

ionization of its constituents [27]. The two main ionization mechanisms in laser plasmas are the ionization by inelastic collisions of electrons with atoms and the direct multiphoton ionization of atoms due to bound–free transitions of atomic electrons. The ionization rate in the case of collisional ionization w_c is given by [27]

$$w_c \approx \frac{\nu_{in}\xi_{os}}{I_i} \tag{3}$$

where ν_{in} is the frequency of inelastic collision, I_i is the ionization energy and ξ_{os} is the electron oscillation energy given by [27]

$$\xi_{os} = 0.093\lambda^2 I \text{ (eV)} \tag{4}$$

Here λ is the wavelength of the laser light and I is the power density (W cm^{-2}) at the focal spot. In the case of direct photoionization, however, the ionization rate is given by [27]

$$w_n \approx w_0 n^{3/2}\left(\frac{\xi_{os}}{I_i}\right)^p \tag{5}$$

where $p = I_i/\hbar\omega$ is the number of absorbed quanta. It is clear from the above equations that the ionization rate is dependent on the laser power densities through the electron oscillation energy. Although the collisional ionization rate has a weak dependence on the laser power density, the ionization rate due to the multiphoton processes is strongly dependent on the power densities. In the present case $\hbar\omega = 1.17$ eV for 1.06 μm radiation, which is very much smaller than the ionization potentials of any of the constituent atoms inside the plasma. The first ionization energies for different constituents of the YBCO plasma are [37] 6.38 eV (Y), 5.21 eV (Ba), 7.73 eV (Cu) and 13.62 eV (O). As the ionization rate is directly proportional to the electron density, the dependence of the electron density on the laser power density should be the same as that of the ionization rate, except for a change in the proportionality constant. The direct photoionization of any of these atoms requires more than one photon for 1.06 μm radiation.

Fig. 5 shows the double logarithmic plot of the laser power density vs the emission intensity of single ionic lines from Y (3950.36 Å), Ba (3891.78 Å) and Cu (4171.85 Å). One can see that the intensity of these lines grow as I^p, where $p \approx 6$ for Y, 5 for Ba and 6 for Cu at lower power densities but p lies approximately between 1 and 2 at higher power densities. For both Y and Ba the multiphoton energy slightly exceeds the

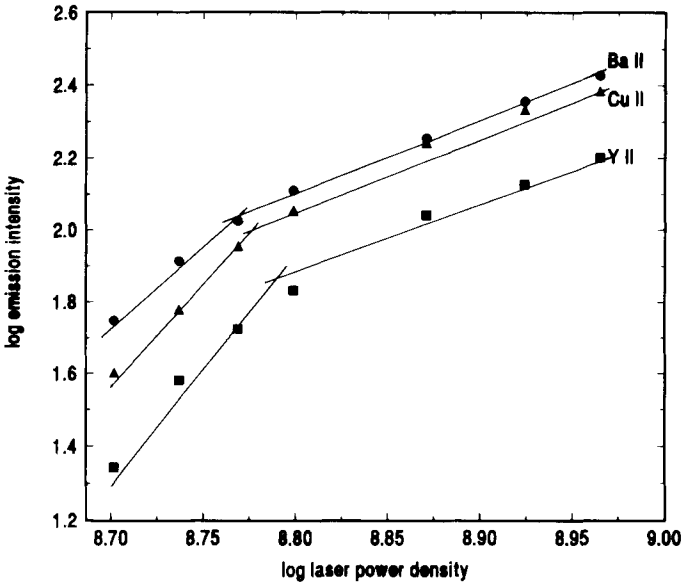

Fig. 5. Variation of the logarithm of the ion emission intensity of first ionized lines: ■, YII (3950.36 Å); ●, BaII (3891.78 Å); ▲, CuII (4171.85 Å); with log laser power density showing multiphoton ionization at low laser power densities and collision induced ionization at higher power densities.

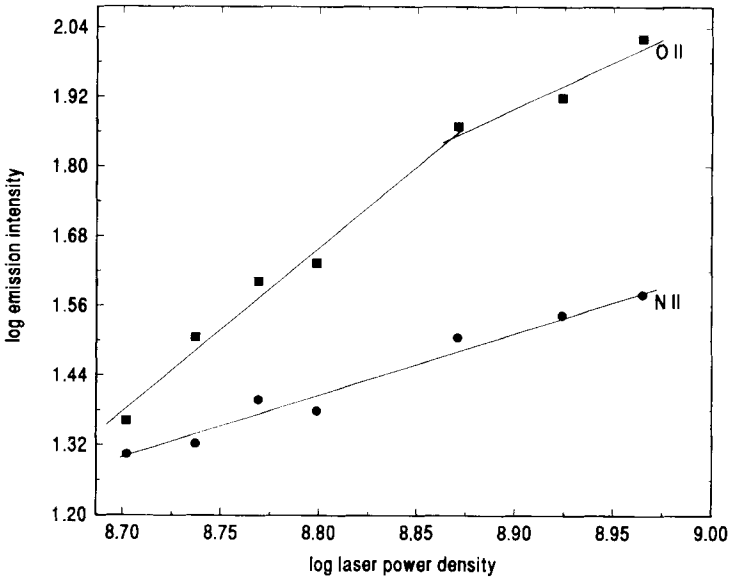

Fig. 6. Plot of logarithm of ion emission intensity for: ■, OII (4072.16 Å); ●, NII (4041.31 Å); indicating the effect of collisional ionization for oxygen and nitrogen within the power density range.

ionization potential, but for Cu it is slightly less than the ionization potential. This effect could be due to the depletion of the neutral atoms inside the plasma, as suggested by several other workers [38,39]. However, from Fig. 6, for N (4041.31 Å) the emission line intensity grows very gradually with p in the range 1–1.5. In this case there is no saturation of the line intensity at higher power densities, indicating that from very low to very high power densities the ionization rate is the same. For oxygen (4072.16 Å), there exists a change in slope in the log–log plot shown in Fig. 6. But the higher slope at low laser power densities does not match with the ionization potential of oxygen. The simultaneous absorption of 12 photons is required for the direct multiphoton photoionization of oxygen, the cross-section for which is very low. There can be a small number of molecules becoming multiphoton photoionized, but the major contribution is from collisional processes. The results in Figs. 4 and 5 show that at low laser power densities the elements present inside the target with comparatively low ionization potentials are multiphoton photoionized, whereas atmospheric nitrogen gets ionized due to collisions throughout the power density range. Emission corresponding to oxygen is stronger than that due to nitrogen because of the additional source of oxygen from the target apart from that present in the atmosphere. At high laser power density the ionization is due to collisions, in the case of species with low ionization potentials (Y, Ba and Cu) also.

For low laser power densities, i.e. in the range 0.55–0.65 GW cm^{-2}, the electron density also varies as $n_e \propto I^p$, where p has values between 6 and 7 (Fig. 4). This supports the fact that multiphoton absorption is a dominant ionization process in this range. $6\hbar\omega = 7.02$ eV is slightly greater than the ionization potentials of Y and Ba. But above 0.65 GW cm^{-2}, the dependence of the electron density on the power density is rather weak, where p ranges from 1 to 2. Here the exponent is close to unity and obviously multiphoton ionization is not likely to be the dominant process. Instead of multiphoton photoionization, collision induced ionization which is weakly dependent on the laser power density is dominant. This means that when a threshold electron number density is exceeded, the number of inelastic collisions between the electrons and the atoms increases and the main ionization mechanism is the collision induced one. The fact that above 0.65 GW cm^{-2} the emission spectrum is rich in singly ionized species with some doubly ionized ones supports the above argument. The higher ionized states should be due to collisions and

not due to photoionization because of the very high ionization potentials, whereas in the case of low laser power densities the dominance of neutral and singly ionized species and the absence of higher ionized states show that the collision dominated processes are negligible. Another reason for the saturation effect in the electron density at higher laser power density is the laser absorption by the plasma near the target surface. This will reduce the effective laser power density available for laser–target interaction. A similar phenomenon has been suggested by other workers [13].

Above the threshold laser power density (0.65 GW cm^{-2}) the trailing part of the laser beam does not penetrate sufficiently into the plasma to cause multiphoton ionization. Before being expanded, the plasma is confined to a region with dimensions characteristic of the etch depth on the target (with typical values of a few μm; see for example refs. [40,41]). During this period the trailing part of the laser pulse interacts with the plasma. Above this threshold value of the laser power density, the electron density present within the etch depth during the period of the laser pulse may exceed the critical density. Hence the laser light is screened off, being absorbed by the plasma.

4. Conclusions

Various aspects of a laser produced plasma in air with laser power densities ranging from 0.55 to 1.5 GW cm^{-2} have been investigated using emission spectroscopy and Michelson interferometry. It is found from the time resolved emission measurements that spectral emission during the formation of the laser plasma is dominated by the plasma continuum, revealing the existence of free electrons and ions in abundance, but some time (typically 55 ns for 0.8 GW cm^{-2}) after the termination of the laser pulse the plasma emission is dominated by atomic and ionic lines. This means that after attaining a maximum emission intensity the plasma begins to cool, during which time various recombination and de-excitation processes control the emission mechanism. From the intensity measurements of various emission lines as a function of laser power density, it can be concluded that at low laser power densities the main ionization mechanism for elements like Y, Ba and Cu constituting the target is multiphoton induced, whereas the main ionization mechanism is collision induced at higher laser power densities. For Cu, though it is present in the target itself, the number of quanta absorbed at low laser power densities is slightly less than that required for multiphoton photoionization. As a result of the high ionization potential, the major ionization mechanism in the case of oxygen atoms happens to be collision induced even though oxygen is present in the target as a major constituent. The emission intensities from species such as N present outside the bulk target show a linear dependence with the laser power density, indicating the existence of collisional ionization processes. Line averaged electron densities were deduced from the interferometric measurements and found to vary from 10^{16} to 2.4×10^{17} cm^{-3} as the laser power density is increased from 0.5 to 1.1 GW cm^{-2}. Plasma temperature was calculated from the integrated line intensities of emission from ionized species and found to be about 1 eV. In conclusion, optical emission spectroscopy and Michelson interferometry were utilized for the investigation of a high density low temperature nanosecond laser produced plasma from the multi-component material $YBa_2Cu_3O_7$ in air at atmospheric pressure.

Acknowledgements

This work was supported by research grants from the Department of Science and Technology (Government of India) and Science, Technology and Environment Department (Government of Kerala). S.S.H. is grateful to CSIR (New Delhi), R.C.I. and C.V.B. to UGC (New Delhi) for research fellowships.

Appendix A

The intensity distribution of the fringe pattern of a Michelson interferometer is given by

$$I(t)=A^2+B^2+2AB\cos[(\phi_A-\phi_B)-\gamma(t)] \quad \text{(A1)}$$

where A and B are the amplitudes and ϕ_A and ϕ_B are the phases of the respective interfering beams and $\gamma(t)$ is the phase difference introduced due to the presence of the plasma. (This derivation is made in accordance

with the arguments given in Monson et al. [42]). The shift in the fringe pattern resulting from this time dependent phase factor can be measured as the voltage change in the output of the photodiode. For the intensity to be very sensitive to small changes in $\gamma(t)$, the operating point is chosen such that $\phi_A - \phi_B = (m + 1/2)\pi$. Then the change in the output voltage of the photodetector $\delta V(t)$ is

$$\delta V(t) \propto 2AB \sin\left[\frac{4\pi}{\lambda}\int_0^l \Delta\mu(t)\mathrm{d}l\right] \tag{A2}$$

where λ is the wavelength of the probe laser beam, l is the lateral extension of the plasma and $\Delta\mu(t)$ is the change in refractive index due to the presence of the plasma. When the phase difference $(\phi_A - \phi_B)$ is taken through a phase change of π, i.e., the operating point is moved from the bright to the dark fringe center, the corresponding difference in intensities $(I_{max} - I_{min})$ will be proportional to $4AB$ in the absence of the plasma. With a linear response for the photodetector, the corresponding voltage difference $(V_{max} - V_{min})$ denoted by V is proportional to $4AB$. Therefore, from Eq. (A2)

$$\gamma(t) = \sin^{-1}\left(\frac{2\Delta V}{V}\right) \tag{A3}$$

Assuming negligible absorption and light scattering at the probe wavelength, the index of refraction μ of the plasma is given by [43] $\mu^2 = 1 - (n_e/n_c)$ where n_e is the plasma electron density and n_c is the critical plasma electron density given by $n_c = (\omega^2 m\epsilon_0/e^2)$, where ϵ_0 is the permittivity of free space, m is the electron mass, e is the electron charge and ω is the angular frequency of the pump laser radiation. n_c has a typical value of 9.92×10^{20} cm^{-3} for the Nd:YAG laser wavelength (λ = 1.06 μm). Also, when the critical density $n_e/n_c \ll 1$

$$\gamma(t) \cong \frac{e^2}{mc\omega\epsilon_0}\int_0^l n_e \mathrm{d}l \tag{A4}$$

for path length l in the plasma. Therefore the line averaged electron density from Eq. (A4) is

$$\bar{n}_e \cong \frac{k\gamma(t)}{\lambda l} \tag{A5}$$

where $k \cong 1.778 \times 10^{12}$ cm^{-1}. The phase factor $\gamma(t)$ in Eq. (A5) is found experimentally using Eq. (A3).

References

[1] D.L. Pappas, K.L. Saenger, J.J. Cuomo and R.W. Dreyfus, J. Appl. Phys., 72 (1992) 3966.
[2] D. Dijikkamp, T. Venkatesan, X.D. Wu, S.A. Shaheen, N. Jisrawi, Y.H. Min-Lee, W.L. McLean and M. Croft, Appl. Phys. Lett., 51 (1987) 619.
[3] L. Lynds, V.R. Weiberger, G.G. Peterson and H.A. Krasinski, Appl. Phys. Lett., 52 (1988) 320.
[4] D.S. Misra and S.B. Palmer, J. Appl. Phys., 68 (1990) 1403.
[5] Y. Watanabe, Appl. Phys. Lett., 64 (1994) 1295.
[6] J. Wild, P. Engst, S. Civis, J. Pochyly and J. Pracharova, Appl. Phys. Lett., 60 (1992) 1747.
[7] H. Jiang, A.J. Drehman, R.J. Andrews and J.A. Horrigan, Appl. Phys. Lett., 65 (1994) 3132.
[8] C.M. Davis, H.H. Telle, D.J. Montgomery and R.E. Corbett, Spectrochim. Acta Part B, 50 (1995) 1059.
[9] W. Pietsch, B. Dubreuil and A. Briand, Appl. Phys. B, 61 (1995) 267.
[10] P.E. Dyer, R.D. Greenough, A. Issa and P.H. Key, Appl. Phys. Lett., 53 (1988) 534.
[11] C.E. Little and P.G. Browne, Chem. Phys. Lett., 134 (1987) 560.
[12] L.C. Jensen, S.C. Langford, J.T. Dickinson and R.F. Addleman, Spectrochim. Acta Part B, 50 (1995) 1501.
[13] R.K. Singh and T. Narayan, Phys. Rev. B, 41 (1990) 8843.
[14] K.P.J. Reddy, Pramana, 46 (1996) 153.
[15] S.S Harilal, R.C. Issac, C.V. Bindhu, V.P.N. Nampoori and C.P.G. Vallabhan, J. Appl. Phys., 80 (1996), 3561.
[16] K.H. Wu, R.C. Wang, S.P. Chen, H.C. Lin, J.Y. Juang, T.M. Uen and Y.S. Gou, Appl. Phys. Lett., 69 (1996) 421.
[17] Y.-M. Kim, W.-J. Lee and H.-G. Kim, Thin Solid Films, 279 (1996) 140.
[18] J.R. Ho, C.P. Grigoropoulos and J.A.C. Humphrey, J. Appl. Phys., 79 (1996) 7205.
[19] H. Nishikawa, M. Kanai and T. Kawai, Jpn. J. Appl. Phys., 35 (1996) L-425.
[20] M. Hemmerlin and J.M. Mermet, Spectrochim. Acta Part B, B51 (1996) 579.
[21] Z. Andreic, B. Flenc-Bartolie and H.J. Kunze, Phys. Scr., 48 (1993) 331.
[22] S. Eliezer, H. Hora, E. Kolka, F. Green and H. Szichma, Laser Particle Beams, 13 (1995) 441.
[23] R.E. Walkup, J.M. Jasinski and R.W. Dreyfus, Appl. Phys. Lett., 48 (1986) 1690.
[24] X.L. Mao, M.A. Shannon, A.J. Fernandez and R.E. Russo, Appl. Spectrosc., 49 (1995) 1054.
[25] R.F.G. Meulenbroeks, M.F.M. Steenbakkers, Z. Qing, M.C.M. van de Sanden and D.C.M. Schram, Phys. Rev. E, 49 (1994) 2272.
[26] T. Okada, N. Shedamary, J. Nakaujama and M. Maeda, Appl. Phys. Lett., 60 (1994) 941.
[27] E.G. Gamaly, Laser Particle Beams, 12 (1994) 185.
[28] W.C. Stwalley and J.T. Bahns, Laser Particle Beams, 11 (1993) 185.
[29] E.G. Gamaly and R. Dragila, Phys. Rev. A, 42 (1990) 929.

[30] S.S. Harilal, R.C. Issac, C.V. Bindhu, G.K. Varier, V.P.N. Nampoori and C.P.G. Vallabhan, Pramana, 46 (1996) 145.
[31] S.S. Harilal, P. Radhakrishnan, V.P.N. Nampoori and C.P.G. Vallabhan, Appl. Phys. Lett., 64 (1994) 3377.
[32] D.B. Geohegan, Thin Solid Films, 220 (1992) 138.
[33] G. Bekefi, Principles of Laser Plasmas, Wiley Eastern, New York, 1976, p. 590.
[34] H.R. Griem, Plasma Spectroscopy, McGraw Hill, New York, 1964.
[35] D.B. Geohegan, in D.B. Chresey and G.K. Hubler (Eds.), Pulsed Laser Deposition of Thin Films, John Wiley & Sons, New York, 1994, p. 138.
[36] A.P. Thorne, Spectrophysics, Chapman and Hall, 1974, p. 386.
[37] Handbook of Chemistry and Physics, CRC, Boca Raton, FL, 1988.
[38] S.L. Chin, N.R. Isenor and M. Young, Phys. Rev., 188 (1969) 7.
[39] C.O. Park, H.W. Lee, T.D. Lee and J.K. Kim, Appl. Phys. Lett., 52 (1988) 368.
[40] R.A. Neifeld, E. Potenziana, W.R. Sinclair, W.T. Hill III, B. Turner and A. Rinkas, J. Appl. Phys., 69 (1991) 1107.
[41] F.C. Burns and S.R. Cain, J. Phys D: Appl. Phys., 29 (1996) 1349.
[42] B. Monson, R. Vyas and R. Gupta, Appl. Opt., 28 (1989) 2554.
[43] L. Spitzer, Physics of Fully Ionized Gases, Interscience, New York, 1956.